

Article

Design of a 94 GHz Millimeter-Wave Four-Way Power Combiner Based on Circular Waveguide Structure

Siyu Tu , Jinsong Liu, Tianyi Wang , Zhengang Yang and Kejia Wang *

Wuhan National Laboratory for Optoelectronics, School of Optical and Electronic Information, Huazhong University of Science and Technology, Wuhan 430074, China; tusiyu_hust@163.com (S.T.); jsliu@hust.edu.cn (J.L.); tianyiwang@vip.163.com (T.W.); mikleyang@163.com (Z.Y.)

* Correspondence: kjwang@hust.edu.cn

Abstract: This paper introduces a four-way power combiner operating in the 94 GHz millimeter-wave based on spatial power combining technology. The four millimeter-waves with Gaussian beams are combined in the waveguide, increasing the output power. The combiner is composed of five circular waveguides connected by four long and narrow coupling slots. Four sub-waveguides are separately connected to four input ports and one main waveguide is connected to a common output port. The TE_{11} -mode is used as the input mode, which has two vertical and horizontal polarization directions. Four sub-waveguides are respectively input corresponding to polarization directions TE_{11} -wave with Gaussian beams. The power of TE_{11} -wave is transmitted to the main waveguide by the coupling slots, combined in the main waveguide, and output with the common port. We analyze the combiner and verify the availability of the design structure by numerical stimulation with CST MWS (Microwave Studio) software. The power-combining efficiency can be over 97%, and the output beams remain Gaussian beams with nearly fourfold increased power. The proposed model provides technological approaches for power combiner application in millimeter-wave.

Keywords: power-combining efficiency; Gaussian beams; circular waveguide; TE_{11} -mode



check for updates

Citation: Tu, S.; Liu, J.; Wang, T.; Yang, Z.; Wang, K. Design of a 94 GHz Millimeter-Wave Four-Way Power Combiner Based on Circular Waveguide Structure. *Electronics* **2021**, *10*, 1795. <https://doi.org/10.3390/electronics10151795>

Academic Editor: Giovanni Andrea Casula

Received: 1 July 2021
Accepted: 24 July 2021
Published: 27 July 2021

Publisher's Note: MDPI stays neutral with regard to jurisdictional claims in published maps and institutional affiliations.



Copyright: © 2021 by the authors. Licensee MDPI, Basel, Switzerland. This article is an open access article distributed under the terms and conditions of the Creative Commons Attribution (CC BY) license (<https://creativecommons.org/licenses/by/4.0/>).

1. Introduction

In general, the output power from a single power source is limited. However, higher power is required in order to have a larger action radius, stronger anti-jamming capability, and better transmission quality. Higher power generation is not possible from a single source. Therefore, the power combiner is a key component to increase output power in the microwave and millimeter-wave system. Many scholars have developed power combiners with spatial power-combining technology based on waveguide structures. Xin Cao proposed a two-way power combiner, operated on 30 GHz with 800 mw of power and 78.9% of combining efficiency [1]. Xiao et al. proposed a two-curved channel compact power combiner operating in X band that significantly reduces the impact of reflected waves in interactive areas [2]. Recently, most research for power combiner has been focused on microwave [3,4] and low-frequency millimeter-wave [5]. These have problems of too large size and low power, respectively.

High-frequency millimeter-wave has the advantage of narrow beams, strong penetrability, high resolution, and better anti-interference, displaying well-applied prospects in communications [6–9], imaging [10,11], and radar [12,13]. Simultaneously, high-frequency millimeter-waves have a shorter wavelength, which could effectively reduce the size of components and provide more benefits in terms of system miniaturization. The power of a single source in high-frequency millimeter-wave is limited by material properties. The power combiners in low frequency millimeter-wave with high-power output have a large system size. The high-frequency millimeter-wave power combiners are preferable to low frequency ones in anti-jamming, transmission quality, imaging resolution, and precision

tracking radar ability [14]. Consequently, a power combiner is worthy of important research in the field of high-frequency millimeter-wave systems. At present, there are few studies on high-power combiners in high-frequency millimeter-wave systems. The main difficulty is how the structure of the combiner can support high-power combination and output. Some power combiners in high-frequency millimeter-wave systems [15–17] based on circuit power combining technology are usually capable of carrying tens of watts.

Therefore, a feasible four-way power combiner that combines four millimeter-waves with Gaussian beams by spatial power combining technology based on circular waveguide structures was proposed in 94 GHz. Spatial power combining technology [18–21], based on waveguide structures, has been investigated in the fields of microwave for a long time, which can realize efficiently combining of multiplexing power. Compared with circuit power combining technology, spatial power combining technology is more suited to high power combining. The power capacity of the combiner can reach MW level. Circular waveguide has the characteristic of low loss and dual polarization, often employed in antenna feeder and microwave resonance cavity [22–24], also forming the output cavity of the microwave tubes [25]. Furthermore, circular cylinder waveguides are easy to fabricate in the four-way power combiner [15]. Moreover, the power handling capacity of a circular cylinder waveguide is larger than that of a rectangular waveguide in the same cross-section area [26]. Consequently, the design structure of the combiner is based on a circular cylinder waveguide. On the basis of coupled mode theory, the four millimeter-waves with Gaussian beams could be transmitted and combined in the waveguide by designing a favorable structure. The output power could be increased fourfold, and the output beams remain Gaussian beams. In particular, the combiner has high isolation and high power-combining efficiency with low-loss in the 94 GHz millimeter-wave. In addition, the structure of a power combiner is compact, symmetrical, and relatively miniaturized, which will be more convenient in some applications.

The remainder of the paper is organized as follows. In Section 2, we employ coupled mode theory to design the four-way power combiner, and provide a detailed introduction to the structure of this combiner. In Section 3, we performed numerical simulation analysis on this combiner with CST MWS simulation software, and investigated the influence of the physical mechanism of the combiner for power-combining efficiency. We investigate the optimum dimensions of the structure of the combiner to realize the highest power-combining efficiency. Finally, our conclusions are summarized in Section 4.

2. Theory and Model

2.1. Theory

The following is the principle of the four-way power combiner. According to coupled wave theory, the waves will couple with each other during the transmission process when mutually parallel waveguides are adjacent to each other. While there is a coupling structure between two adjacent waveguides, power exchange occurs during wave transmission between waveguides. The coupling equation is as follows:

$$\frac{dE_a}{dz} = iK_{ab}E_b \exp[i(k_a - k_b)z] + iC_aE_a \quad (1)$$

$$\frac{dE_b}{dz} = iK_{ba}E_a \exp[i(k_b - k_a)z] + iC_bE_b \quad (2)$$

$$k_a - k_b = \Delta k \quad (3)$$

For a single mode, effective coupling can occur when the propagation constants are equal:

$$C_a = C_b \quad (4)$$

Assuming that waveguide-b has a single mode wave propagation and waveguide-a has no wave propagation at $z = 0$ (port 4), $E_b(0) = E_{b0}$, $E_a(0) = 0$. The power of the

two waveguides is $|E_a(z)|^2$ and $|E_b(z)|^2$, respectively. The schematic is shown in Figure 1. According to power conservation conditions,

$$\frac{d}{dz} (|E_a(z)|^2 + |E_b(z)|^2) = 0 \quad (5)$$

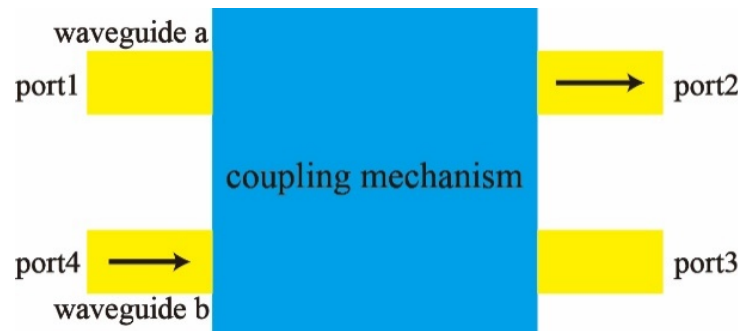


Figure 1. Coupling mechanism.

The powers of the waveguide-a and the waveguide-b are as follows:

$$P_a(z) = P_{b0} \frac{K^2}{[K^2 + (\Delta k)^2]} \sin^2 \left([K^2 + (\Delta k)^2]^{1/2} z \right) \quad (6)$$

$$P_b(z) = P_{b0} \left(1 - \frac{K^2}{[K^2 + (\Delta k)^2]} \sin^2 \left([K^2 + (\Delta k)^2]^{1/2} z \right) \right) \quad (7)$$

When $[K^2 + (\Delta k)^2]^{1/2} z = \pi/2$, the $P_a(z)$ reaches the maximum with realizing the maximum power conversion between the two waveguides. The excitation power input to port 4 is transmitted to waveguide-a by favorable coupling structures and output from port 2. Port 1 and port 3 have basically no power output. The power of waveguide-b is almost completely transmitted into waveguide-a, and the maximum power conversion efficiency is as follows:

$$\eta = \frac{P_a(z)}{P_{b0}} = \frac{K^2}{K^2 + (\Delta k)^2} \quad (8)$$

When $\Delta k = 0$, complete power conversion is realized.

Among the transmission modes of a circular waveguide, the TE_{11} -mode is the fundamental mode of circular waveguide and suitable mode for antenna. The TE_{11} -mode has vertical and horizontal polarization directions, and the coupling coefficients in the two polarization directions are very different. Furthermore, the TE_{11} -mode could cause direct radiation into the atmosphere. According to the orthogonal polarization mode theory, the polarization direction of the TE_{11} -mode is associated with the structural direction of the designed coupling slot when coupling the TE_{11} -wave from one waveguide to another. When the designed coupling slot structure is appropriate for coupling the vertical polarization TE_{11} -wave, the vertical polarization TE_{11} -wave input to one waveguide can be completely coupled to another waveguide by the coupling slot, but the horizontal polarization TE_{11} -waves input to one waveguide can be rarely coupled to another waveguide. When the designed coupling slot structure is appropriate for coupling the vertical polarization TE_{11} -wave, the horizontal polarization TE_{11} -wave input to one waveguide can be completely coupled to another waveguide by the coupling slot, but the vertical polarization TE_{11} -waves input to one waveguide can rarely be coupled to another waveguide. These principles are shown in Figures 2 and 3 by numerical stimulation software CST.

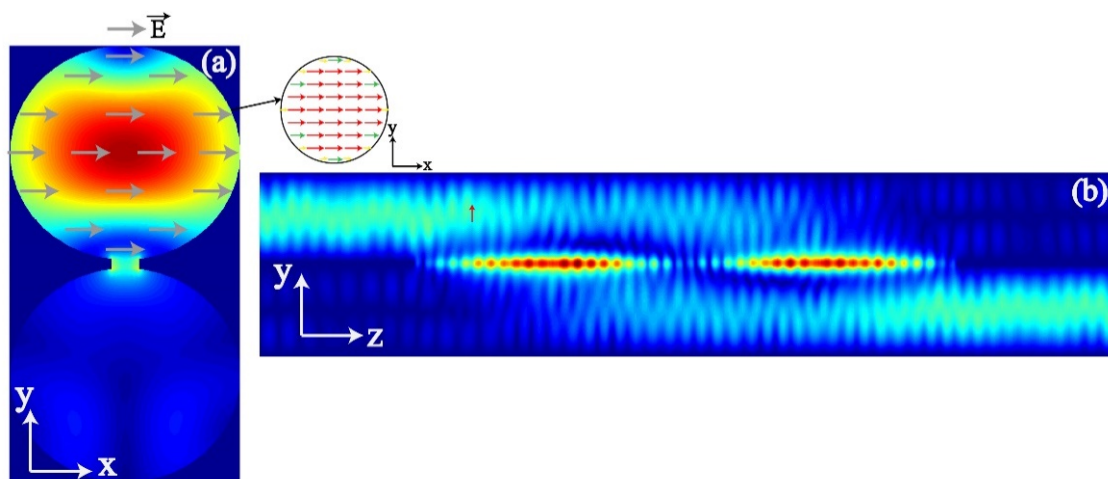


Figure 2. Horizontal polarization wave inputting: (a) coupling slot structure direction and the transverse electric field and (b) longitudinal electric field (YZ cross section).

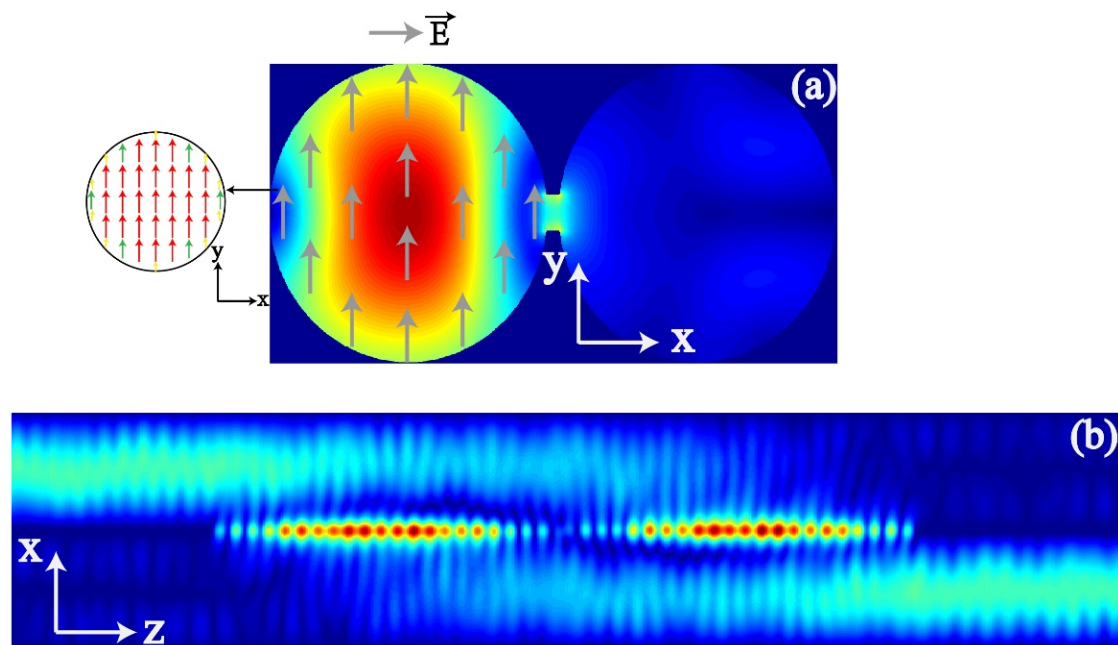


Figure 3. Vertical polarization wave inputting: (a) coupling slot structure direction and the transverse electric field and (b) longitudinal electric field (XZ cross section).

In Figures 2 and 3, the two identical waveguides are connected by a coupling slot. Significantly, the connected direction of the two waveguides by the coupling slot is different, and the transverse and longitudinal electric-field distributions are shown. In Figure 2a, the horizontal polarization TE_{11} -wave with Gaussian beams is input to a single waveguide, and the connected direction of two waveguides by the coupling slot is the y-direction. In Figure 2b, it can be clearly seen that the great majority of power of the horizontal polarization TE_{11} -wave input to one waveguide is transmitted to another waveguide by the coupling slot. Similarly, the vertical polarization TE_{11} -wave with Gaussian beams is input to one waveguide, and the direction of the coupling slot connected with two waveguides is the x-direction, as shown in Figure 3. The great majority of power of the vertical polarization TE_{11} -wave input to one waveguide is transmitted to another waveguide. In Figure 4, the connected direction of the coupling slot between two waveguides is the x-direction, and the two waveguides are input horizontal and vertical polarization TE_{11} -wave with Gaussian beams simultaneously, respectively. It can clearly be seen that the vertical polarization

TE_{11} -waves are mostly coupled to another waveguide by the coupling slot. Nevertheless, the structure of the coupling slot is not appropriate for coupling the horizontal polarization TE_{11} -wave. Hence, the horizontal polarization TE_{11} -wave is absolutely transmitted in its own waveguide and is isolated from another waveguide. Fang et al. [27] proposed a two-way power combiner using circular waveguides based on spatial power combining technology with this theory in 9–10 GHz. The input mode of the microwave is the vertical polarization TE_{11} -wave, which realized the transmission and combination of 3 GW power in engineering.

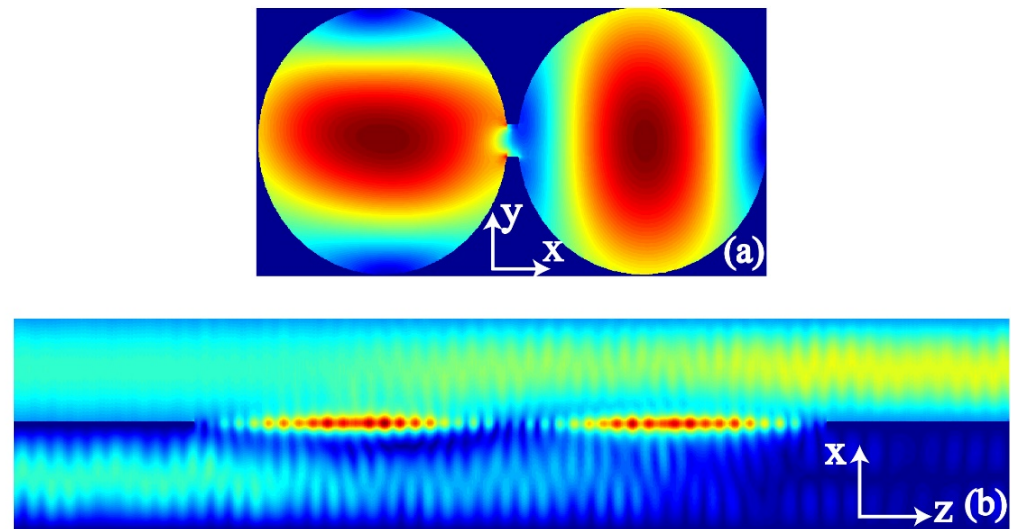


Figure 4. Horizontal and vertical polarization wave simultaneously inputting: (a) coupling slot structure direction and the transverse electric field and (b) longitudinal electric field (XZ cross section).

2.2. Model

Figure 5a is the designed 3D (three-dimensional) structure of the four-way millimeter-wave power combiner in this paper. The center is the main-waveguide, and the four sub-waveguides are symmetrically located above, below, left, and right of the main-waveguide. The combiner is a centrally symmetrical structure at the XY cross section. The main-waveguides are closely connected with each sub-waveguide by four coupling slots. Figure 5b,c show the detailed structure parameters of the combiner. Figure 5b is the XZ cross section of the combiner. The radius R and length of the five waveguides are equal, while the length of the four coupling slots is also equal. The distance W between the main-waveguide and sub-waveguides is equal. The position of the main waveguide along the z -direction relative to the sub-waveguides is 15 mm apart. In the z -direction, the starting position of the coupling slot is 5 mm away from the starting position of the main waveguide, the bottom of the coupling slot is 5 mm from the bottom of the sub-waveguide and 20 mm from the bottom of the main waveguide. Figure 5c is the XY cross-section structure of the combiner. The width of the four coupling slots is L_w . The starting position of the sub-waveguides is $z = 0$ mm along the z -direction. The center of the main-waveguide is $x = 0$ mm and $y = 0$ mm in XY coordinates. The main waveguide is the power-combining and common output channel, and the four surrounding sub-waveguides are the input channels. Port 1 and port 2 are input vertical polarization TE_{11} -waves with Gaussian beams. Port 3 and port 4 are input horizontal polarization TE_{11} -waves with Gaussian beams.

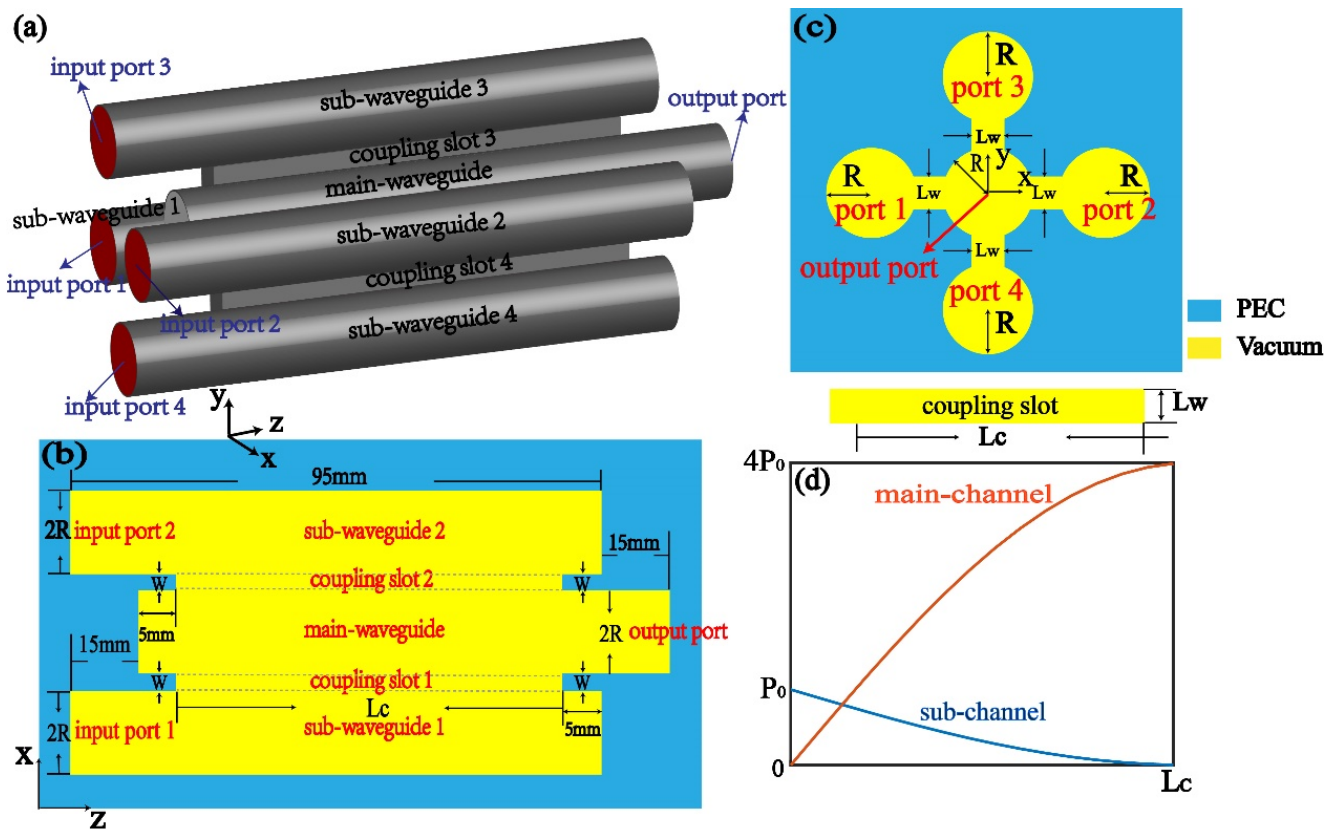


Figure 5. (a) Combiner 3D structure, (b) longitudinal structure view, (c) transverse structure view, and (d) theoretical power variation.

L_c is the designed coupling length of the four coupling slots. When L_c reaches a certain value, the entire power can theoretically be transmitted from the sub-waveguides to the main-waveguide. Four TE_{11} -waves are coupled to the main-waveguide by four coupling slots, and combined in the main channel. This combiner was input identical power, so the variation of theoretical power in the main waveguide is as follows:

$$P_{total} = 4P_0 \frac{K^2}{[K^2 + (\Delta k)^2]} \sin^2 \left([K^2 + (\Delta k)^2]^{1/2} z \right) \quad (9)$$

Theoretical variation of the power of one sub-waveguide and main-waveguide is shown in Figure 5d, and the final output power is $4P_0$ at the common output port. This structure could theoretically increase the output power by four times, which is a solution to the limited application of a single power millimeter-wave source.

3. Results

To verify the availability of the model proposed in Section 2, we use 3D CST MWS with the finite integral method to numerically design and investigate the four-way power combiner in 94 GHz millimeter-wave. The numerical simulation frequency band is 93–95 GHz, and the center frequency is 94 GHz. Port 1 and port 2 are input 1 MW power of vertical polarization TE_{11} -waves with Gaussian beams, respectively. Port 3 and port 4 are input 1 MW power of horizontal polarization TE_{11} -waves with Gaussian beams, respectively. For the operating frequency, the circular waveguide’s radius R is optimized to 3.6 mm. The distance W between the main-waveguide and sub-waveguides is 2 mm. According to the coupled wave theory, the power transmission degree is closely related to the width L_w and length L_c of the coupling slot. The narrower the L_w , the longer the L_c required for the entire power transmission when the size of radius R is constant. Consequently, we

have indicated the influence of L_w and L_c on power-combining efficiency under decidedly circular waveguide radius. Finally, we present the numerical simulation results of the four-way power combiner in 94 GHz millimeter-wave.

3.1. The Influence of the Coupling Length L_c

The coupling slot length L_c is critical when the combiner employs long and narrow coupling slots for power transmission. Suppose that L_c is shorter, only part of the power could be transmitted into the main waveguide, while part of the power remains in the sub-waveguide. Nevertheless, the too long coupling slot length L_c is not beneficial for device miniaturization. Therefore, we have investigated an appropriate length of L_c . In accordance with the radius R of circular waveguides, we first choose an integer value 3 mm from R as the coupling width L_w . Figure 6 shows the power-combining efficiency at different L_c . In Figure 6a, the L_c ranges from 40 mm to 90 mm, and the interval is 5 mm. In Figure 6b, the L_c ranges from 65 mm to 75 mm, and the interval is 1 mm. When L_c is 70 mm, the highest power-combining efficiency is 97.05%. The power-combining efficiency decreases when L_c is more than 70 mm. As a result of operating on the high frequency millimeter-wave condition, some higher order modes are generated in waveguides. The power carried by higher order modes is transmitted back to the sub-waveguides because of the too long coupling slots, so the power-combining efficiency is reduced. In the subsequent studies of the combiner, the coupling slot length L_c is 70 mm in all cases.

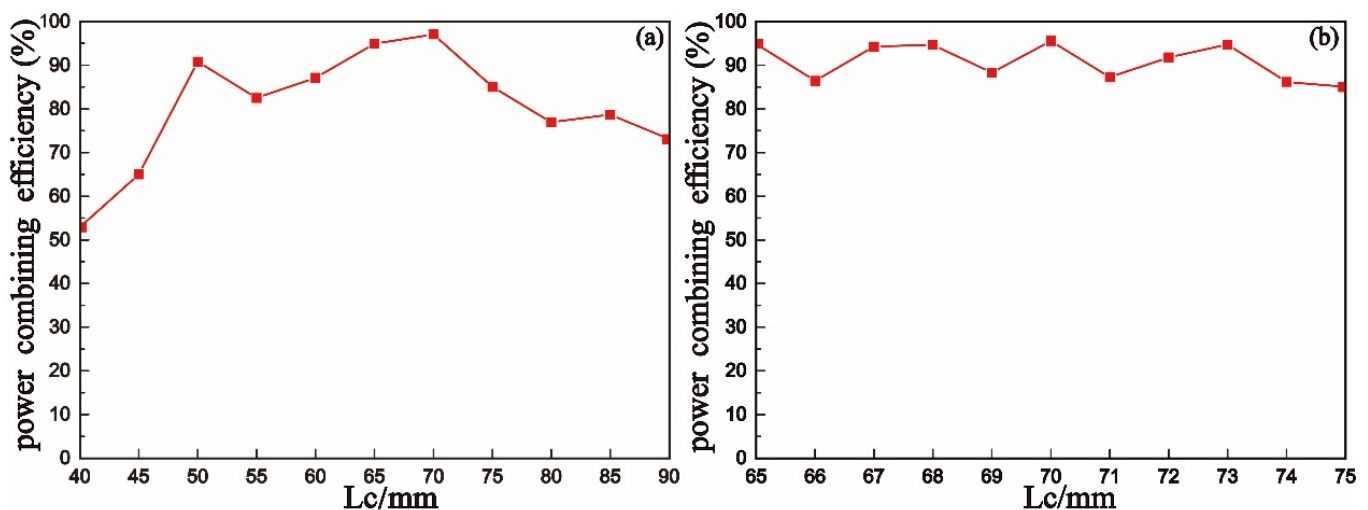


Figure 6. Power-combining efficiency under different coupling slot lengths L_c : (a) the L_c with large interval, (b) the L_c with small interval.

3.2. The Influence of the Coupling Length L_c

For invariant waveguide radius R and coupling slot length L_c , numerical simulation research demonstrates that there is an upper limit of the coupling slot width L_w to achieve higher transmission efficiency. Excessive coupling slot L_w width could cause serious damage to the boundary conditions of circular waveguides. If the L_w is greater than this value, the transmission power would decrease. The coupling slots' length L_c is 70 mm in all cases. The coupling slot width L_w ranges from 2 mm to 4 mm, and the interval is 0.2 mm. Figure 7 shows the power-combining efficiency at different L_w . As L_w ranges from 2.6 mm to 3.2 mm, the power-combining efficiency can reach about 97%. The highest power-combining efficiency is 97.41% when L_w is 2.8 mm. For L_w is 4 mm, the power-combining efficiency drops to only 52.30%. L_w has the greatest influence on the power-combining efficiency compared with the coupling slot length L_c , and a slight difference could lead to great variation of power-combining efficiency.

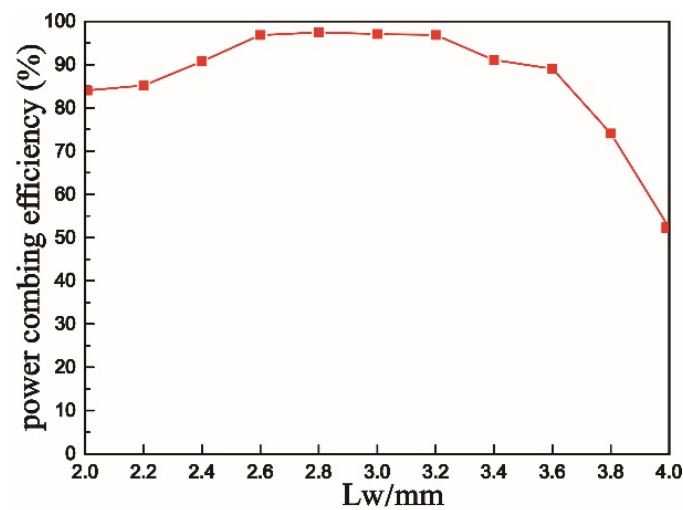


Figure 7. Power-combining efficiency under different coupling slot width L_w .

3.3. Stimulation Field

The dimensions of the combiner with the highest power-combining efficiency are as follows: $R = 3.6$ mm, $W = 2$ mm, $L_w = 2.8$ mm, and $L_c = 70$ mm. As shown in Figure 8, this is the electric and power field distribution of the combiner. In Figure 8a,c, they are the electric and power field distribution in the main waveguide and the sub-waveguides 1 and 2 (XZ cross section). In Figure 8b,d, they are the electric and power field distribution in the main waveguide and the sub-waveguides 3 and 4 (YZ cross section). It could be clearly observed that the polarization TE_{11} -waves input in the four sub-waveguides are largely coupled into the main-waveguide by the coupling slots, and only a small part of the power remains in the sub-waveguides. Figure 9 shows the electric field distribution of the XY cross section of the combiner. Figure 9a is the electric field distribution of the vertical polarization TE_{11} -waves with Gaussian beams of the sub-waveguides 1 and 2 and the horizontal polarization TE_{11} -waves with Gaussian beams of the sub-waveguides 3 and 4 of the initial position ($z = 0$ mm) of the combiner. Figure 9b shows that the majority of the power is still in the sub-waveguides and a very small part of the power begins to be coupled into the main waveguide at the beginning of the coupling slots. Figure 9c shows that the power of sub-waveguides coupled to the main-waveguide happens by the coupling slots, and a portion of the power remains in the sub-waveguides at the middle of the coupling slot ($z = 60$ mm). Additionally, we can see the combination phenomenon of the four waves in the main waveguide. Figure 9d shows that most of the powers are coupled to the main waveguide near the bottom of the coupling slots ($z = 89$ mm). Only very small amount of power is retained in the four sub-waveguides. Two horizontal and two vertical TE_{11} -waves are basically completely combined in the main waveguide. Figure 9e shows the electric field distribution at the common output port of the main waveguide. Two horizontal and two vertical polarization Gaussian beams are basically completely combined in the main waveguide, and the output beams are still Gaussian beams with higher power. The maximum electric field and power of the combiner are 1.355×10^7 V/m and 3.996×10^{11} V \times A/m², respectively.

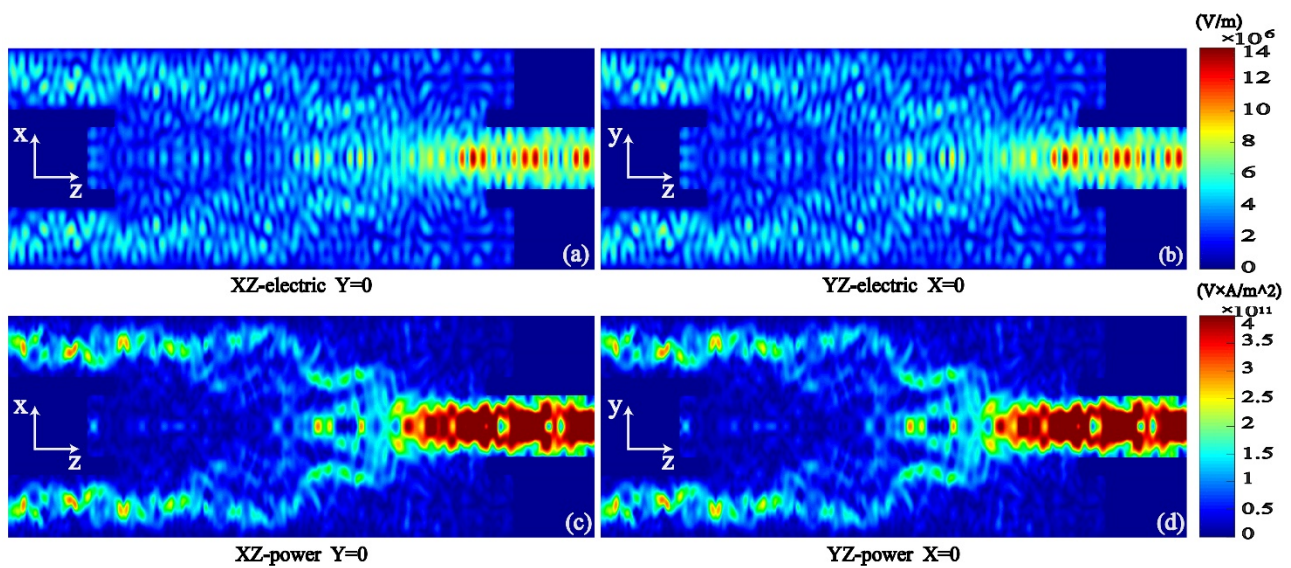


Figure 8. (a) Electric field distribution on XZ cross section, (b) electric field distribution on YZ cross section, (c) power distribution on XZ cross section, (d) power distribution on XZ cross section.

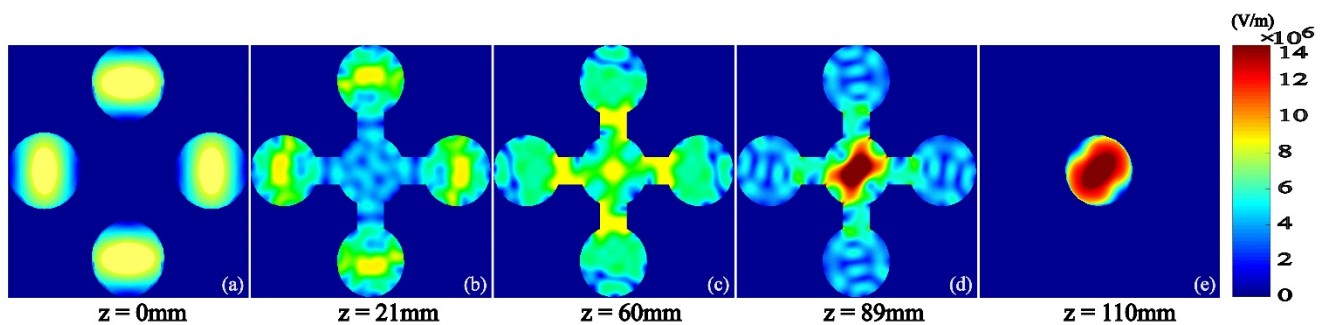


Figure 9. Transverse electric field distribution at different z (a) $z = 0$ mm, (b) $z = 21$ mm, (c) $z = 60$ mm, (d) $z = 89$ mm, and (e) $z = 110$ mm.

The transmission coefficient from input port 1 to output port S_{51} is -0.11 dB, and the transmission coefficient from other input ports to the output ports are identical because the four sub-waveguides are symmetrical with the main waveguide. The reflection coefficient from input port S_{11} is -39.95 dB, and other input ports have identical reflection coefficient owing to symmetry. The transmission coefficient between two input ports S_{12} is -37.95 dB when the two input ports are in the same direction. The transmission coefficient between two input ports S_{13} and S_{14} is 57.67 dB when the two input ports are in different directions. Owing to the symmetry of the structure of the power combiner, the transmission coefficients between other two input ports are identical with port 1.

In the combiner, z from 20 mm to 90 mm is the coupling area. The blue line in Figure 10a is the variation of normalization center power of the sub-waveguide 1 ($x = 0$, $y = 0$ mm) along the z direction. The normalization center power of the sub-waveguides gradually decreases to a small value of the coupling region. The orange line in Figure 10a is the variation of the normalization central power of the main waveguide along the z direction, and the normalization central power of the main waveguide gradually increases in the coupling region. In Figure 10b, the blue line and the orange line are the variation of normalization power of sub-waveguide 1 and main waveguide, respectively, along the z direction. As the four sub-waveguides are centrally symmetrical with the main waveguide in the XY cross section, the variation of the power of four sub-waveguides, which are not to be described in detail, is identical. This can also be observed and demonstrated by Figures 8 and 9. Figure 10c,d are the variation of normalization center power of waveguides

along the x direction and the y direction, respectively. X from -12.8 mm to -5.6 mm is the region of sub-waveguide 1, x from -3.6 mm to 3.6 mm is the region of the main waveguide, x from 5.6 mm to 12.8 mm is the region of sub-waveguide 2. X from -5.6 mm to -3.6 mm and from 3.6 to 5.6 mm are the regions of coupling slot 1 and 2, respectively. Y from 5.6 mm to 12.8 mm is the region of sub-waveguide 3, y from -3.6 to 3.6 mm is the region of the main waveguide, and y from -12.8 mm to -5.6 mm is the region of sub-waveguide 4. Y from 3.6 mm to 5.6 mm and from -5.6 mm to -3.6 mm are the regions of coupling slot 3 and 4, respectively. The two blue lines are the variation of normalization central power of the combiner at the beginning of the coupling slots. It can be observed that the power of the four sub-waveguides is high and the power of the main waveguide is very small. The two orange lines are the variation of normalization central power of the combiner at the end of the coupling slot. The power of the main waveguide becomes extremely large, and the power of the sub-waveguides becomes very small. In addition, the normalization center power of the main waveguide at the bottom of the coupling slot is approximately four times the power of one sub-waveguide at the beginning of the coupling slots. The power of the common output port is 3.8963 MW. The power-combining efficiency of the power combiner is 97.41% in 94 GHz millimeter-wave. The polarization TE_{11} -waves with Gaussian beams of the four sub-waveguides are all coupled into the main waveguide by the coupling slots connected to the main waveguide. Only less than 4% of the power remains in the sub-waveguides or is lost in transmission, realizing the highest power-combining efficiency and promoting the output power.

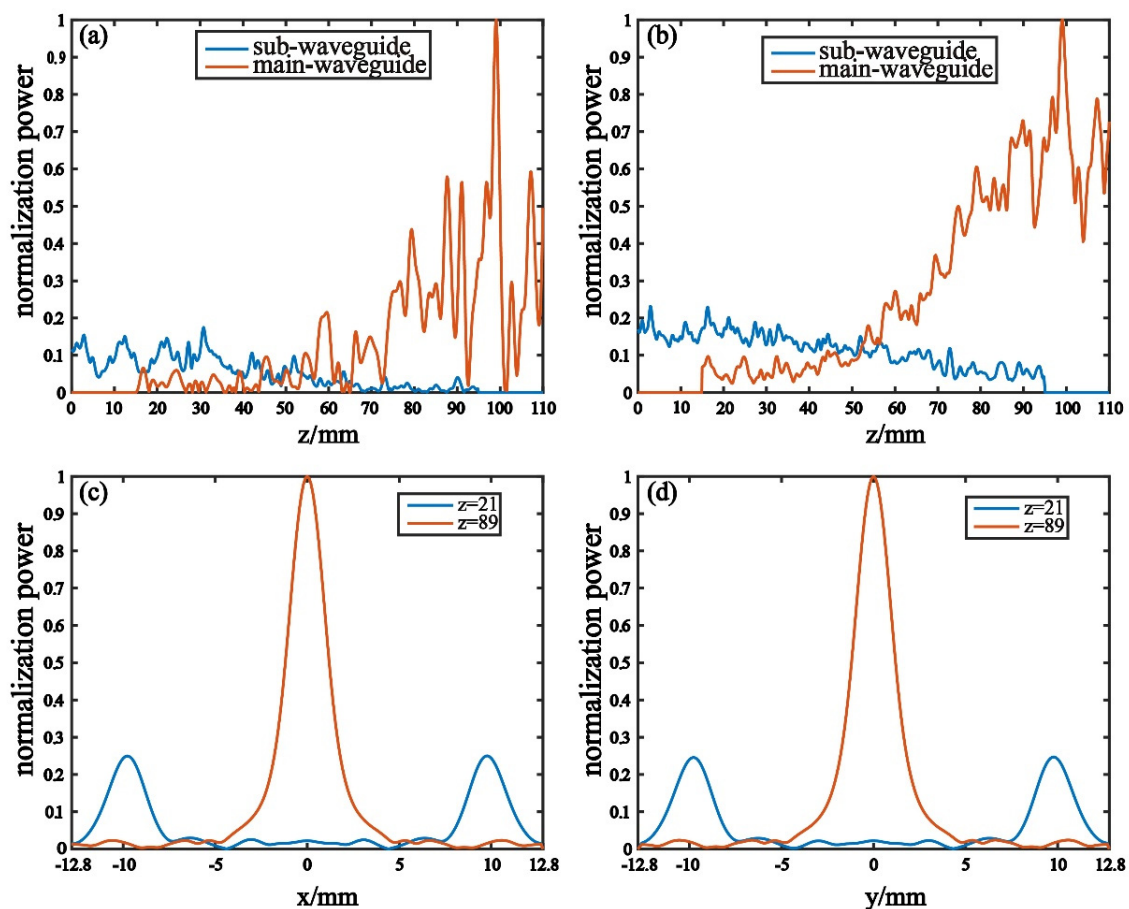


Figure 10. (a) The normalization power of the center of the main waveguide and sub-waveguide 1 along the z direction ($x = 0$, $y = 0$ mm); (b) the normalization power of the main waveguide and sub-waveguide 1 along the z direction; (c) the blue line and the orange line are the variation of the center power of the combiner along the x direction at the beginning and at the end of the coupling slot, respectively; and (d) the blue line and the orange line are the variation of the center power of the combiner along the y direction at the beginning and at the end of the coupling slot, respectively.

The electric field distributions in Figures 8 and 9 show that the four TE₁₁-waves input to four input ports are largely coupled from sub-waveguides to the main waveguide. The power measured at the output port also shows that most of the power is combined and output in the main waveguide. It is observed that the variation of normalization power of sub-waveguides and main waveguide in Figure 10a,b is roughly consistent with the variation of theoretical power in Figure 5d. It is proved that the model is a feasible method.

4. Discussion

Several combiners with large size or low power in microwave and low frequency millimeter-wave are introduced in the Introduction section. Compared with these power combiners, the four-way power combiner in 94 GHz could increase output power by four times and has a structure with a small size, which is conducive to system miniaturization. The carried power capacity can reach MW level using circular waveguides based on spatial power-combining technology. A long and narrow coupling slot is employed, which facilitates the power coupled from sub-waveguides to the main waveguide. In addition, the sub-waveguides are located in the upper, lower, left, and right directions of the main-waveguide. The TE₁₁-waves of different polarization directions are input. The structure has good isolation between sub-waveguides to achieve high power-combining efficiency. Nevertheless, the size of the coupling slot is small, which needs to be more precise in the production. A slight variation of the size of the coupling slot might lead to a large variation of power-combining efficiency. When the processing procedure is imperfect or waveguides are inhomogeneous, the polarization direction of the TE₁₁-mode could be rotated.

In engineering application, the 94 GHz signal source can be connected to the W₁₀ rectangular waveguide port through the coaxial. Because the design of the four-way power combiner is a circular waveguide port, a rectangular-to-circular converter is required. The 94 GHz signal source generally transmits millimeter-wave signal with TE₁₀ or TM₁₀ mode. It can be connected to the input ports of the four-way power combiner of the manuscript through over-mode bent waveguide, which can realize the mode conversion to generate the TE₁₁ mode. The mode converter can be used to ensure the propagation of a single mode.

5. Conclusions

This paper presents a four-way power combiner in 94 GHz high frequency millimeter-wave. The power combiner is designed with a symmetrical structure by circular waveguides and coupling slots. We employ the coupled mode theory and the coupling coefficient difference of the two vertical and horizontal polarization directions TE₁₁-mode. Four-way TE₁₁-waves with Gaussian beams are coupled to the main waveguide by the corresponding coupling slot structure. Then, the four millimeter-waves are combined in the main channel and output with a common port, the power-combining efficiency can be over 97%, and output power is increased by nearly four times. Furthermore, the combined output beams remain Gaussian beams. The four-way power combiner is a solution to the power limitation of a single millimeter-wave source, which can realize 3.8693 MW high-power combination and output in the high-frequency millimeter-wave.

Author Contributions: Conceptualization, S.T.; methodology, S.T.; software, S.T.; validation, S.T.; formal analysis, S.T.; investigation, S.T.; resources, S.T.; data curation, S.T.; writing—original draft preparation, S.T.; writing—review and editing, S.T.; visualization, S.T.; revised, K.W., J.L., T.W. and Z.Y. All authors have read and agreed to the published version of the manuscript.

Funding: This research was funded by National Defense Pre-Research Foundation of China, No. 61422160107.

Acknowledgments: Thanks to my tutor for his careful guidance.

Conflicts of Interest: The authors declare no conflict of interest.

References

1. Cao, X.; Tang, Z.; Wang, F. A two-way power amplifier based on waveguide spatial power-combing technique in Ka-band. *Electromagnetics* **2016**, *36*, 447–456. [[CrossRef](#)]
2. Xiao, R.Z. Power combiner with high power capacity and high combination efficiency for two phase-locked relativistic backward wave oscillators. *Appl. Phys. Lett.* **2015**, *107*, 1–4. [[CrossRef](#)]
3. Li, J.; Huang, W.; Zhu, Q.; Xiao, R.; Shao, H. Influence of a falling edge on high power microwave pulse combination. *Phys. Plasmas* **2016**, *23*, 073104. [[CrossRef](#)]
4. Guo, L. A waveguide magic-T with coplanar arms for high-power solid-state power combing. *IEEE Trans. Microw. Theory Technol.* **2017**, *65*, 2942–2952. [[CrossRef](#)]
5. Garcia-Perez, J.A.; Kosmopoulos, S.; Goussetis, G. A Compact 12-Way Slotted Waveguide Power Combiner for Ka-Band Applications. *IEEE Microw. Wirel. Compon. Lett.* **2017**, *27*, 135–137. [[CrossRef](#)]
6. Seeds, A.J.; Williams, K.J. Microwave Photonics. *J. Light. Technol.* **2006**, *24*, 4628–4641. [[CrossRef](#)]
7. Miller, S.E.; Tillotson, L.C. Optical and transmission research. *Appl. Opt.* **1966**, *5*, 1538–1549. [[CrossRef](#)] [[PubMed](#)]
8. Lim, C.; Nirmalathas, A.; Bakaul, M.; Lee, K.-L.; Novak, D.; Waterhouse, R. Mitigation strategy for transmission impairments in millimeter-wave radio-over-fiber networks [Invited]. *J. Opt. Netw.* **2009**, *8*, 201–214. [[CrossRef](#)]
9. Beas, J.; Castanon, G.; Aldaya, I.; Aragon-Zavala, A.; Campuzano, G. Millimeter-Wave Frequency Radio over Fiber Systems: A Survey. *IEEE Commun. Surv. Tutor.* **2013**, *15*, 1593–1619. [[CrossRef](#)]
10. Yeom, S.; Lee, D.-S.; Son, J.-Y.; Jung, M.-K.; Jang, Y.; Jung, S.-W.; Lee, S.-J. Real-time outdoor concealed-object detection with passive millimeter wave imaging. *Opt. Express* **2011**, *19*, 2530–2536. [[CrossRef](#)]
11. Fetterman, M.R.; Grata, J.; Jubic, G.; Kiser, W.L.; Visnansky, A. Simulation, acquisition and analysis of passive millimeter-wave images in remote sensing applications. *Opt. Express* **2008**, *16*, 20503. [[CrossRef](#)] [[PubMed](#)]
12. Cui, C.; Kim, S.-K.; Song, R.; Song, J.-H.; Nam, S.; Kim, B.-S. A 77-GHz FMCW Radar System Using On-Chip Waveguide Feeders in 65-nm CMOS. *IEEE Trans. Microw. Theory Tech.* **2015**, *63*, 3736–3746. [[CrossRef](#)]
13. Sarabandi, K.; Park, M. A radar cross-section model for power lines at millimeter-wave frequencies. *IEEE Trans. Antennas Propag.* **2003**, *51*, 2353–2360. [[CrossRef](#)]
14. Song, K.; Fan, Y.; He, Z. Broadband Radial Waveguide Spatial Combiner. *IEEE Microw. Wirel. Compon. Lett.* **2008**, *18*, 73–75. [[CrossRef](#)]
15. Zhang, F.; Song, K.; Fan, M.; Fan, Y. All-Metal-Waveguide Power Divider with High Power-Combining Efficiency. *J. Infrared Millim. Terahertz Waves* **2016**, *37*, 258–266. [[CrossRef](#)]
16. Li, J.; Li, L.; Lü, L.; Shi, H.; Huo, H.; Zhang, A. Four-way waveguide power divider design for W-band applications. *Int. J. RF Microw. Comput. Eng.* **2018**, *28*, e21242. [[CrossRef](#)]
17. Wei, T. Analysis and design of high-power and efficient, millimeter-wave power amplifier systems using zero degreecombiners. *INT J. Electron* **2018**, *105*, 1–11.
18. Chang, K.; Sun, C. Millimeter-Wave Power-Combining Techniques. *IEEE Trans. Microw. Theory Tech.* **1983**, *31*, 91–107. [[CrossRef](#)]
19. Takechi, O.; Shinohara, N.; Matsumoto, H. Spatial power combing oscillator array with band elimination filter connection method for microwave power transmission. *Electron. Commun. Jpn.* **2005**, *88*, 1–9.
20. Xie, Z.M.; Zhang, R. Gain factor of horn array feed offset parabolic cylindrical reflector antenna for spatial power combining. *Microw. Opt. Technol. Lett.* **2010**, *52*, 1742–1747. [[CrossRef](#)]
21. Xie, X.; Zhao, X.; Liu, X. A waveguide-based spatial power combing module at higher millimeter-wave frequency. *J. Infrared. Milli. Terahz. Waves* **2013**, *34*, 299–307. [[CrossRef](#)]
22. Franco, M.J. A high-performance dual-mode feed horn for parabolic reflectors with a stepped-septum polarizer in a circular waveguide. *IEEE Antennas Propag. Mag.* **2011**, *53*, 142–146. [[CrossRef](#)]
23. Lai, G.; Liang, R.; Zhang, Y.; Bian, Z.; Yi, L.; Zhan, G.; Zhao, R. Double plasmonic nanodisks design for electromagnetically induced transparency and slow light. *Opt. Express* **2015**, *23*, 6554–6561. [[CrossRef](#)] [[PubMed](#)]
24. Huang, Y.; Min, C.; Veronis, G. Broadband near total light absorption in non-PT-symmetric waveguide-cavity systems. *Opt. Express* **2016**, *24*, 22219–22231. [[CrossRef](#)]
25. Elfrgani, A.; Seidfaraji, H.; Yurt, S.C.; Fuks, M.I.; Schamiloglu, E. Power Combiner for High Power Cerenkov Devices. *IEEE Trans. Plasma Sci.* **2016**, *44*, 2268–2271. [[CrossRef](#)]
26. Xiao, R.; Deng, Y.; Song, Z.; Li, J.; Sun, J.; Chen, C. An All Circular Waveguide Four-Way Power Combiner With Ultrahigh-Power Capacity and High Combination Efficiency. *IEEE Trans. Plasma Sci.* **2018**, *46*, 1–5. [[CrossRef](#)]
27. Fang, J.Y. An X band synthesizer for a few hundred megawatt level power microwaves. *Acta Phys. Sin.* **2011**, *60*, 088402-1–088402-7.